



A 30-year-old diesel tank: fungal-dominated biofilms cause local corrosion of galvanised steel



Ruben Gerrits¹, Biwen An Stepec², Ralph Bäßler¹, Roland Becker¹, Matthias Dimper¹, Ines Feldmann¹, Kira L. Goff³, Jens Günster¹, Andrea Hofmann¹, René Hesse¹, Sarah Kirstein⁴, Ulrich Klein¹, Tatjana Mauch¹, Meina Neumann-Schaal⁴, Ozlem Ozcan¹, Nicole M. Taylor³, Julia Schumacher^{1,5}, Yin Shen³, Heike Strehlau¹, Matthias Weise¹, Jacqueline Wolf⁴, Andrey Yurkov⁴, Lisa M. Gieg³ ✉ & Anna A. Gorbushina^{1,5} ✉

The increased use of biodiesel is expected to lead to more microbial corrosion, fouling and fuel degradation issues. In this context, we have analysed the metal, fuel and microbiology of a fouled diesel tank which had been in service for over 30 years. The fuel itself, a B7 biodiesel blend, was not degraded, and—although no free water phase was visible—contained a water content of ~60 ppm. The microbial community was dominated by the fungus *Amorphotheca resiniae*, which formed thick, patchy biofilms on the tank bottom and walls. The tank sheets, composed of galvanised carbon steel, were locally corroded underneath the biofilms, up to a depth of a third of the sheet thickness. On the biofilm-free surfaces, Zn coatings could still be observed. Taken together, *A. resiniae* was shown to thrive in these water-poor conditions, likely enhancing corrosion through the removal of the protective Zn coatings.

Hydrocarbon fuel is long known to be biodegradable¹. Microbial contamination of fuel systems, even though often dubbed “fuel algae”, consists mostly of bacteria and fungi^{2–4}, with archaea being reported rarely⁵. In general, these communities are dominated by aerobic species^{6,7}. However, anaerobic microorganisms like methanogens, nitrate-reducing bacteria, and sulphate-reducing bacteria (SRB) were also observed to grow on aerated (bio)diesel⁵, indicating the presence of local anoxic zones in fuel tanks. Marks et al.⁸ showed that diesel components found in the metal ballasts of marine ships can be utilised both aerobically and anaerobically, with these processes occurring in succession. Note that in many fuel systems, it is not always clear whether specific organisms metabolise the hydrocarbon chains of the fuel or the fuel additives, or whether they are only surviving in fuel tank systems⁹.

Apart from the breakdown of hydrocarbons, microbial growth in fuel systems can cause other environmental and economic issues related to fouling or the corrosion of the metal infrastructure^{9–11}. This is especially the case for diesel fuels⁹. Fouling, attributed primarily to fungi and extracellular polymeric substance (EPS)-producing bacteria⁹, can cause operational failures by blocking the flow of fuels by filter plugging, or by disabling pumps, valves or tank gauges¹². Corrosion of the fuel tanks will lead to

leakage and is thought to be mostly caused by SRB⁹. Indeed, the SRB *Desulfoglaeba alkanexedens* was shown experimentally to cause carbon steel corrosion when grown on diesel¹³, but the same can be said of various fungi^{14–16}, or the aerobic heterotroph *Bacillus clausii*¹⁷. Known microbial corrosion mechanisms are (among others) organic acid production, direct electron transfer, use of intermediate electron carriers like H₂, Fe(II) oxidation, or H₂ production via hydrogenases^{18–20}.

Fouling issues in fuel systems have resulted in the development of mitigation strategies like good maintenance practices (e.g., cleaning, drainage of water)¹², and the application of biocides²¹. These are aided by several detection and monitoring approaches ranging from general detection kits based on microbial growth on agar or the formation of black ferrous sulphide by SRB²², or immunofluorescence²³, to quantitative polymerase chain reaction (qPCR)^{24,25} tests to detect the presence of specific contaminants.

One recent development related to society's quest for renewable energy that drastically increased the relevance of these biofouling processes is the rising production and use of biodiesel based on fatty acid methyl esters (FAME). Not only did the production of biofuels increase by a factor of nine from 2000 to 2020, the proportion of biodiesel (including hydrotreated vegetable oil) as a percentage of the total biofuel production experienced a

¹Bundesanstalt für Materialforschung und -prüfung, Berlin, Germany. ²Norwegian Research Centre, Bergen, Norway. ³University of Calgary, Calgary, Canada.

⁴Leibniz Institute DSMZ - German Collection of Microorganisms and Cell Cultures, Braunschweig, Germany. ⁵Freie Universität Berlin, Berlin, Germany.

✉ e-mail: imgieg@ucalgary.ca; anna.gorbushina@bam.de

tenfold increase in the same timeframe²⁶. Its consumption is mainly taking place in the EU (18 billion litres), Asia (mainly Indonesia, 11 billion litres), Latin America (mainly Brazil, 10 billion litres), and North America (8 billion litres) (data from 2019, including hydrotreated vegetable oil)²⁶. This booming use is expected to further enable fungi and bacteria to cause fouling, fuel degradation, and corrosion¹². The reason is twofold: biodiesel has a higher saturation moisture content²⁷ and is more biodegradable^{4,5,28} compared to conventional diesel. Methanogenic communities, for instance, were shown to have higher methane production when grown on blends with a higher biodiesel content⁵, whereas fungi degraded a higher fraction of FAME than alkanes, when both had an equal chain length¹⁵. Several studies, moreover, noted a community shift upon increasing the biodiesel content^{5,29}, with Schleicher et al.⁶ showing that fungi dominated the community at higher biodiesel contents. The parallel increase in the use of ultra-low sulphur diesel (ULSD), however, neither resulted in a community shift nor in a change in anaerobic metabolism³⁰ and seemingly can be ignored with respect to the abovementioned failures.

Whether such biodiesel-related effects actually cause more diesel tank failures through corrosion remains uncertain. An indication is, however, given by a report on the corrosion prevalence of underground diesel storage tanks (UST), which revealed that 83% of the studied tanks exhibited moderate to severe corrosion, presumably through microbial activity³¹. The report further mentions that, starting in 2007, observations were made of severe corrosion in the upper vapour space, a timing which coincides with the introduction of biodiesel, but also ULSD and an increase in retailers selling diesel³¹. The in situ incubation of carbon steel coupons in such biodiesel storage tanks, moreover, revealed the presence of a diverse bacterial population and one dominant fungal species (identified as *Paecilomyces dactylethromorphus*³²) whose abundance correlated with the corrosion of the coupons³³.

In this context, we were offered a diesel tank of a camper van which had been in use for over 30 years, and which failed due to fouling of the fuel gauge. Initial non-destructive testing revealed the presence of patchy biofilms composed of a diverse bacterial community and a fungal community dominated by one species: *Amorphotheca resinae* (Supplementary Fig. 1). This fungus, better known as the kerosene, diesel or creosote fungus, can degrade multiple pure cyclic and linear hydrocarbons^{34,35}, kerosene³⁶ and (bio)diesel¹⁴ (Gerrits et al., under review) and is therefore a ubiquitous coloniser of various hydrocarbon-containing systems^{37,38}. Furthermore, the production and intracellular accumulation of hydrocarbons (mostly pristane and hexadecane) have been observed as well³⁹. Nevertheless, experimental studies have shown that *A. resinae* was not able to enhance the corrosion rate of carbon steel when grown on (bio)diesel in other studies¹⁴ (Gerrits et al., under review). To determine whether the microbial community inhabiting the fouled diesel tank also had any corrosive effects on the carbon steel material, we undertook a multidisciplinary approach to further assess the microbiological composition, chemical environment (including pH, water content, diesel composition), and material (e.g., corrosion features) underneath biofilms and on bare surfaces in various locations in the tank. Given the initial identification of *A. resinae* as a dominant organism in the diesel tank, we were also interested in understanding whether this organism thrived in such environments solely due to its known diesel-degrading abilities, or whether other factors may have also contributed to its prevalence in this system and in diesel tanks in general.

Results

General description of the opened diesel tank

Non-destructive testing of the fouled diesel tank carried out in 2021 and 2022 showed the appearance of wall-attached deposits which were assumed to be biofilms (Supplementary Fig. 1a). Samples, containing brown flocs, were aseptically collected from the bottom of the diesel tank and near the top of the diesel layer during the non-destructive testing events and subject to amplicon sequencing for both prokaryotes (16S) and the fungi (ITS2). These analyses revealed a diverse prokaryotic community and the dominance of the eukaryotic fungus *A. resinae* (Supplementary Fig. 1b). Anaerobic,

microaerophilic and aerobic enrichment cultures for prokaryotes have so far not resulted in any isolated strain. In contrast, successful culturing of such biomass (flocs) sampled in 2022 led to the isolation of 3 distinct strains of *A. resinae* that were tested for their corrosivity of carbon steel when incubated with glucose or B7 biodiesel (Gerrits et al., in review). With glucose, *A. resinae* caused uniform general corrosion of carbon steel, while when grown on biodiesel, the fungus seemed to protect the steel.

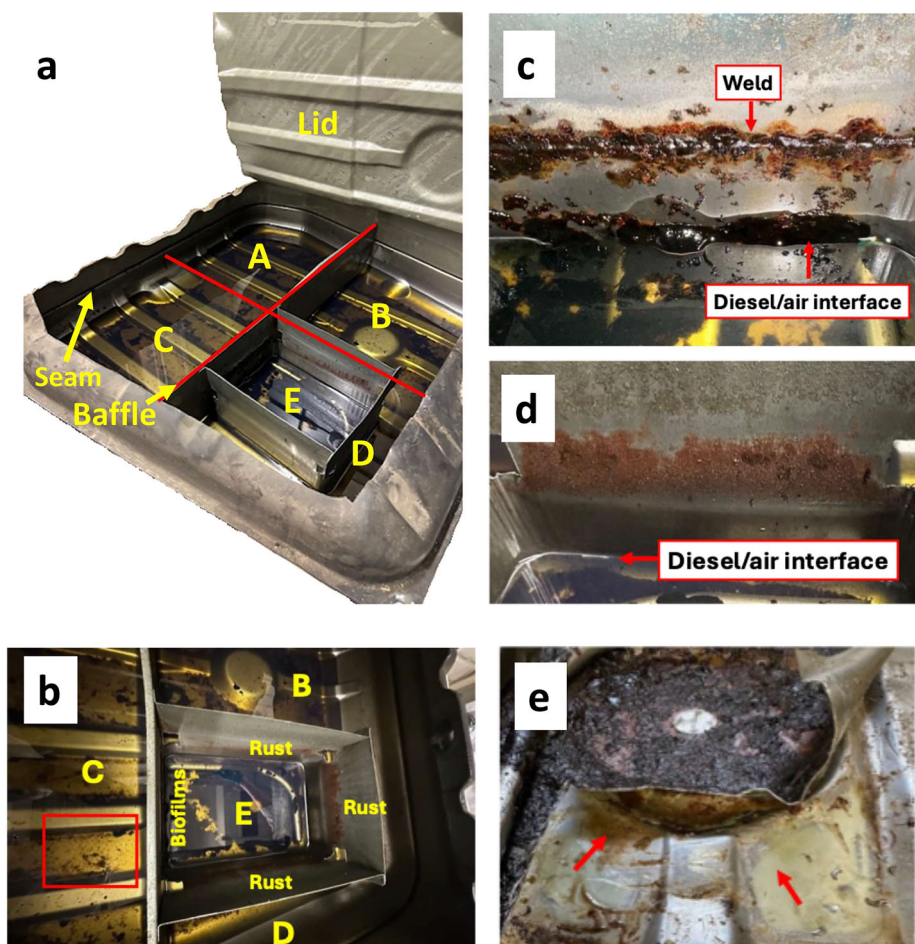
Given these mixed results, we subsequently carried out a more extensive analysis of the fouled diesel tank to better understand the effects that this fungus and other microbial community members inhabiting the tank may have had on the metal surface. The top part of the tank was cut open around the perimeter, creating a lid. The bottom sections of the tanks were arbitrarily designated A to E as indicated in Fig. 1a. Compartment E, a separate section within the larger tank, was the site of the fuel gauge, which had fouled, leading to the failure of the tank. The primary samples collected as 'background' samples, e.g., those that did not show visible evidence of flocs, debris, or biofilm included the lid (designated 'lid'), the bottom of compartment A (i.e., a section with no attached biofilm, designated 'bottom in A'), and the baffle in section D (designated 'baffle in D') (Fig. 1a). The primary samples collected showing visible evidence of flocs, attached debris, or biofilm included the rust layer on a vertical wall of compartment E (designated 'rust in E', Fig. 1b, d), the lower biofilm at the diesel-air interface in compartment E (designated 'lower biofilm in E', Fig. 1c), the upper biofilm on contact area of compartment E and the baffle (designated 'upper biofilm in E', Fig. 1c), and the area between compartment E and the main tank body (designated 'underneath E', Fig. 1e). Other samples that were subject to some analyses included the seam in section C (designated 'seam'), and loose flocs present in each of the five tank sections (designated 'floc A', 'floc B', etc., Fig. 1a, b).

The diesel layer in the tank was measured to be 23 mm deep, and no free water was visibly observed; nevertheless, select samples of the diesel were analysed by coulometry. This analysis showed that the diesel did contain some low amounts of water, ranging from 53.1 ± 7.6 (1 SD) ppm in the fouled compartment E to 64.1 ± 2.8 ppm H₂O in compartment A (fresh B7 diesel was found to contain 73.7 ± 16.2 ppm H₂O). The diesel in the tank had an estimated pH of 5, similar to a fresh diesel sample (obtained from a local fuel station). Diesel samples collected from the main tank and from compartment E were analysed by gas chromatography equipped with flame ionisation detection (GC-FID) and compared to a fresh diesel sample to determine whether biodegradation of the biodiesel took place. However, no discernible differences in the *n*-alkanes or FAME components were evident between these samples (Supplementary Fig. 2).

Microbial community composition within the diesel tank

Non-destructive sampling of fluids (containing some brown flocs) in the diesel tank in 2021 and 2022 was subject to amplicon sequencing for fungi and bacteria/archaea (Supplementary Fig. 1). As indicated earlier, the results showed the predominance of a single fungal amplicon sequence variant (ASV) of *Amorphotheca resinae*, with a lower relative abundance of another *A. resinae* ASV. Fungi affiliated with *Cladosporium* sp. and *Penicillium* sp. were also identified in these early samples (Supplementary Fig. 1b). A fresh B7 diesel sample (from a local fuel station) showed several additional fungal taxa, not detected in the diesel tank. These included *Malassezia* yeasts, an *Agaricomycetes* sp. and a *Penicillium* sp. Sequencing of the V4-V5 region of the 16S rRNA amplicon showed diverse bacterial taxa also present in the diesel tank, including anaerobic taxa such as *Acetobacterium*, *Desulfovermiculus*, *Geobacteraceae*, and halophiles such as *Halanaerobium* (Supplementary Fig. 1c). Between the 2021 and 2022 sampling events, a shift occurred in microbial community composition wherein the relative abundances of several anaerobic taxa decreased. The 2022 data showed an increased relative abundance of organisms such as *Delftia*, *Enterobacteriaceae*, and *Stenotrophomonas*. The fresh diesel sample also contained many prokaryotic taxa which were not or to a lesser extent detected in the diesel tank samples: e.g., *Flavobacterium* sp., *Methanoregula* sp., and *Thiobacillus* sp. (Supplementary Fig. 1c). Notably, many taxa observed in the fresh diesel

Fig. 1 | Photos of the opened diesel tank and select components that were analysed in this study. **a** An overview of the opened tank, showing the arbitrarily designated compartments, along with the lid, seam, and the baffle that were also subject to various analyses. **b** A top view of a portion of the tank highlighting the features of compartment E. In addition, the red boxed area in compartment C is an example of the brown flocs seen throughout the bottom of the tank. **c** A close-up view of the biofilms observed in compartment E; the deposits at the weld are referred to as the upper biofilm in E, while the deposits at the diesel/air interface is called the lower biofilm in E. **d** An example of one of the rust areas observed in compartment E. **e** Brown and pale-yellow deposits observed underneath compartment E following the dismantling of the tank (referred to as underneath E).



sample from 2022 were also found in the diesel tank sample of 2022 but not in 2021 (Supplementary Fig. 1c). This could be either due to cross-contamination or a shift towards “storage conditions” inside the tank resembling those in a UST.

Upon opening the tank, brown biofilm-like deposits were visible in each compartment of the tank that were either floating in the diesel (flocs) or attached to the steel sheets at the bottom and walls (above and below the diesel level). Samples collected from the biofilms and rust layers evident in compartment E, along with the lid, under compartment section E, the seam in compartment C, and the diesel itself (Fig. 1) were analysed by amplicon sequencing targeting a portion of the 16S rRNA gene for prokaryotes (V4-V5 region) and the ITS2 region for fungal identification.

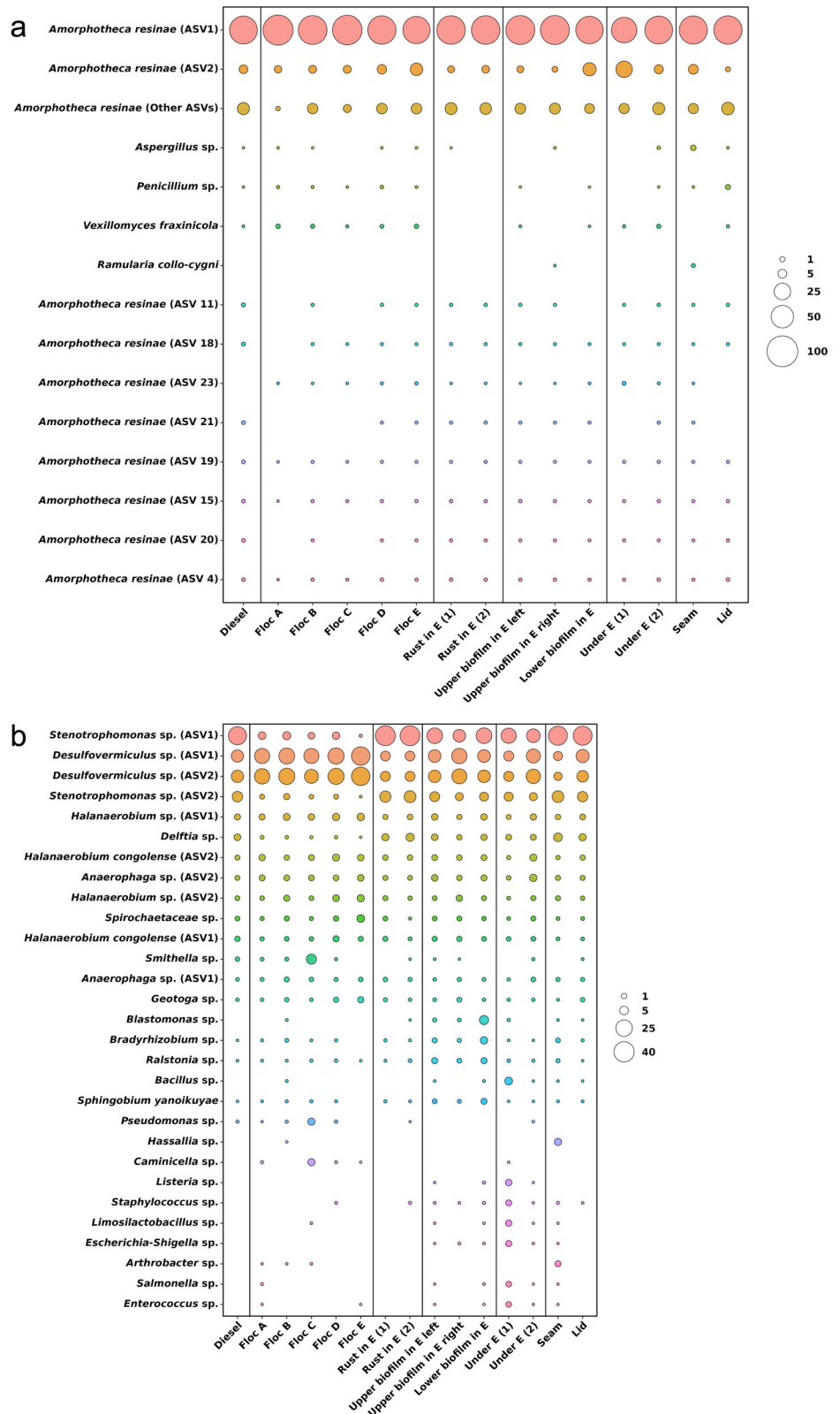
The 2025 fungal community was dominated by multiple ASVs of *A. resiniae* (Fig. 2a), similar to the 2021 and 2022 communities. One *A. resiniae* ASV was dominant across all samples, ranging from 66 to 95% relative abundance of the fungal sequences obtained. A second *A. resiniae* ASV made up the second most abundant fungal taxon, ranging from 1% (lid) to 25% (under E) relative abundance. Many other ASVs identified as *A. resiniae* were also present in the sample. Those that were present in the top 10 most abundant taxa (and occurred at greater than 0.25% relative abundance in at least one sample) are shown as individual ASVs, with all others grouped together as ‘other ASVs’ of *A. resiniae* (Fig. 2a). Although many of the other *A. resiniae* ASVs were individually present in low relative abundances (<1%), this result shows the diversity within this species under these conditions and aligns with the results of Gerrits et al. (under review) who readily isolated three distinct *A. resiniae* strains from this diesel tank. It should be noted, however, that the dominance of *A. resiniae* (and multiple ASVs associated with this taxon) could be due to primer and sequencing biases, which are well-known limitations of amplicon sequencing⁴⁰. Other fungi present at

low relative abundances included *Aspergillus* sp. (0–1.3%—highest in the seam), *Penicillium* sp. (0 to 0.98%—highest on the lid), *Ramularia* sp. (0 to 0.41%—highest in the seam), and *Vexillomyces fraxinicola* (0 to 0.58%—highest in floc E).

Figure 2b presents a summary of the prokaryotic taxa found in all 2025 diesel tank samples. The 10 most abundant taxa for each sample are shown. As with 2021 and 22 samples (Supplementary Fig. 1c), many bacterial taxa were identified, with a decided overlap to previous communities. Notably, ASVs identified as *Stenotrophomonas* and *Desulfovermiculus* were most abundant in the majority of samples, with several other aerobes and anaerobes (including more than one ASV of *Anaerophaga* and *Halanaerobium*) contributing to community structure. Samples taken from loose flocs appeared to contain lower relative abundances of *Stenotrophomonas* but overall were comprised of most of the similar taxa as other samples. Beta diversity analysis (shown as a non-metric multi-dimensional scaling (NMDS) plot in Supplementary Fig. 3) showed some clustering of the loose floc communities, separated from the attached biofilm communities, which also grouped closer to one another. Samples collected and processed in duplicate (such as rust in E) grouped closely in the NMDS analysis.

Metagenomic whole genome analysis of one combined swab of surface-attached biofilms was also conducted to augment amplicon sequencing and allow for further interrogation of the genetic features of the diesel tank community. The metadata of metagenomic whole genome analysis is shown in Supplementary Table 1. Notably, 99.4% of rRNA reads mapped to the 18S rRNA genes, while only 0.6% mapped to 16S rRNA genes, showing the dominance of eukaryotes in the sample. A substantial proportion (77.9%) of the quality-controlled (QC) metagenomic reads mapped to the genome of *A. resiniae* ATCC 22711 (GCA_003019875.1⁴¹). As this method is sensitive towards the genome size of a species, we also

Fig. 2 | Microbial community sequencing results of diesel tank samples. Bubble plots showing the results of **a** ITS (eukaryotes) and **b** 16S rRNA (prokaryotes) gene sequencing of samples collected from various sections of the diesel tank in 2025. The size of the bubbles represents the relative abundances (%) in each sample. The plots were generated based on the top 10 highest relative abundances of ASVs in each sample. For the ITS results, '*A. resiniae*' other ASVs ' contains ASVs that were present at <0.25% relative abundance that were grouped together; numbered '*A. resiniae*' shown are those present at 0.25% relative abundance or greater. Samples rust in E, upper biofilm in E, and under E (underneath E) were sampled and processed in duplicate thus are shown as different samples.

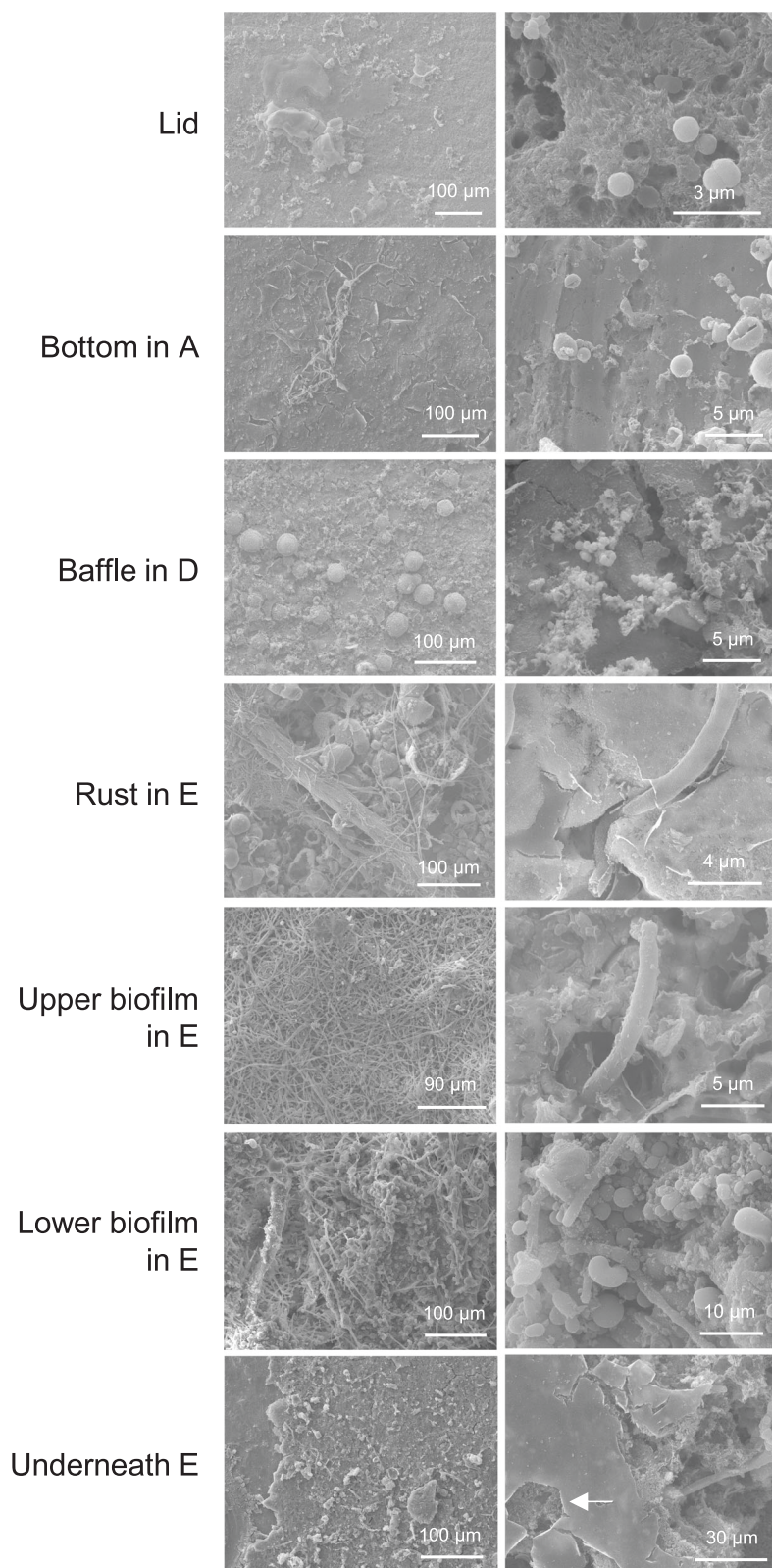


compared the number of 18S reads of *A. resiniae* to the total number of 18S reads. This analysis showed that 82% of the total rRNA belonged to *A. resiniae*, confirming the dominance of this fungus in the diesel tank system by using a different genetic marker.

Sections of the diesel tank were also analysed by environmental scanning electron microscopy (ESEM). Figure 3 shows images of the

surfaces associated with different locations in the tank at broad and smaller scales. Sampled locations that did not have any visible evidence of debris or biomass, including the lid, bottom in A, and baffle in D, revealed the presence of some spherical structures, 3–5 μm in diameter, which possibly represent yeast cells or spores of moulds. The larger round structures (up to 20–30 μm) (Fig. 3, for baffle in D) were observed in direct contact with the

Fig. 3 | ESEM images of samples taken from different locations of the diesel tank. The lid, bottom in A and baffle in D were mostly covered by spherical cells and larger (30 μm in diameter) round cellular structures. The rust in E was composed of large, roundish structures and filamentous fungi. The upper and lower biofilms were composed almost entirely of filamentous fungi together with larger, roundish structures. Underneath E, the hexagonal, wurtzite structures (indicated by the white arrow) are typical of Zn oxides. See Supplementary Fig. 4 for additional SEM images and Supplementary Fig. 5 for EDX analyses.



diesel tank walls and might represent microcolonies containing basidiomycetous yeast cells or chlamydozooids. The mucilage-like appearance of their outer envelopes supports this interpretation, as several detected basidiomycete genera are known to produce EPS capsules.

Sampled areas of compartment E which in contrast showed evidence of debris (rust in E) or biofilms (upper biofilm in E, lower biofilm in E) were

covered with an abundance of fungal hyphae and spherical cells which were notably larger in size than most prokaryotic cells (e.g., larger than 1–2 μm) (Fig. 3), confirming the dominance of fungal biomass in these biofilms and rusty areas. As well observed within the biofilms and on the rust in E sample were large, smooth, roundish structures with diameters ranging from 50 μm to 1 mm (Supplementary Fig. 4). The floating flocs were also mostly

Table 1 | Summary of Zn-associated genes found in the diesel tank metagenome for different taxa based on KEGG orthology (KO)

KO number	-	ko:K07238	ko:K14709	ko:K14713	ko:K14715	ko:K14688	Total hits
Putative function	dimerisation domain of Zn transporter	Zn transporter, ZIP* family (Zn importer)	low-affinity Zn transporter (Zn importer)	Zn transporter (solute family 39)	Zn transporter (solute family 39)	Zrc1/Znt1 (Zn efflux protein/vacuole storage)	
<i>Allantophomopsis cytispora</i>						1	1
<i>Amorphotheca resiniae</i>	1	1	6	2	2	3	15
<i>Amorphotheca resiniae</i> or <i>Exophiala oligosperma</i>						7	7
<i>Exophiala oligosperma</i>	1					5	6
Order Helotiales			1				1
<i>Saxophila tyrrhenica</i>	3		4	1	1	1	10
Unclear	2		4	1		2	9
Unclear, maybe <i>Amorphotheca resiniae</i>				1	1	1	3
Total hits	7	2	15	5	4	19	52

*ZIP = Zn regulated transporter (Zrt)/ Fe regulated transporter (Irt)-like protein.

Table 2 | The depth of the deepest pit observed on a 5 × 5 mm area via scanning white light interferometry

Sample	Maximum pit depth (µm)
Lid	6
Bottom in A	6
Baffle in D	13
Rust in E	55
Upper biofilm in E	95*
Lower biofilm in E	80
Underneath E	9

In general, pits on the metal surface underneath biofilms were much deeper than those on biofilm-free surfaces. Note that this method cannot assess the bottom of deeper pits; thus, the pits on the surface underneath the biofilms may be an underestimation. *A ×20 interferometer objective was used rather than a ×10 objective, which was used for all other samples.

composed of fungal hyphae and cells with a sporadic large (i.e., >50 µm), round structure (Supplementary Fig. 4). Whether these larger, smooth structures are tubercles, fungal sclerotia or have another origin is unknown. Less fungal biomass was evident for a sample taken from underneath E. Rather, this sample and the rust in E sample contained deposits, which were shown by energy-dispersive X-ray spectroscopy (EDX) as being enriched in Zn (Supplementary Fig. 5). This is confirmed by the hexagonal, wurtzite structures in the deposits underneath E, indicative of Zn oxides.

Given the observations made during ESEM-EDX analysis (and the focussed ion beam (FIB) analysis described below) of the presence of Zn or lack thereof under biofilms, we interrogated the metagenome dataset for evidence of Zn-related genes/functions such as Zn transporters, Zn homeostasis, and Zn tolerance. Several Zn transporter orthologs were observed, mostly from *A. resiniae*, and the black microcolonial fungi *Saxophila tyrrhenica* and *Exophiala oligosperma* (Table 1).

Metal analyses

The metal comprising the diesel tank consisted of unalloyed, carbon steel (≤0.22% C, ≤0.30% Ni, ≤0.30% Cr, ≤0.10% Mo) comparable with St 52.4 (1.0581) (as determined via spark-optical emission spectroscopy (OES), Supplementary Table 2). The presence of localised corrosion was investigated by analysis of the profile of metal samples using interferometry and

microscopic analysis of cross-sections after removal of the biofilm and corrosion products. Interferometry delivered profile maps of ~5 mm by 5 mm (Supplementary Figs. 6 and 7), allowing for the estimation of pit depth (as the actual bottom of the deeper pits could not be assessed). The measurable depths of the deepest pits of the metal underneath the upper and lower biofilms in E were 95 µm and 80 µm, respectively, followed by the metal underneath the rust in E at 55 µm (Table 2). The deepest pits in the other samples were generally below 15 µm. Embedding and microscopy of the cross-section of samples from the same locations in the lid, bottom in A, baffle in D, rust in E and upper and lower biofilm and an additional sample from the bottom in A underneath a biofilm showed that the localised corrosion underneath biofilms was more severe (pits of 46, 160 and 270 µm deep, Fig. 4) than estimated by interferometry (Table 2). Interestingly, in one location underneath the lower biofilm in E, where the inner steel sheet of compartment E bended such that direct contact with the diesel and biota on both sides was possible, a hole through the sheet was observed (Fig. 4). Again, just like for interferometry, biofilm-free samples showed more superficial pits. The metal sheet in all locations analysed had a similar thickness, ranging from 710 to 780 µm.

Samples from the same locations were also processed by FIB to visualise and chemically analyse the entire metal-biofilm interface as a cross-section. The images and selected chemical maps of the rust in E, the upper biofilm in E, and the baffle in D samples are shown in Fig. 5 for C, O, Fe, and Zn and in Supplementary Fig. 8 for Cr, Mn, and Pt. Those for the lower biofilm in E, bottom in A and lid samples are shown in Supplementary Fig. 9 and Supplementary Fig. 10. Note that all samples were covered by a protective Pt layer (Supplementary Figs. 8 and 10) and that we only compared the cross-section areas of the different samples. The metal substrate was always enriched in Fe with (for some samples) local inclusions of Mn. An approximately 10 µm thick layer enriched in Zn, O and occasionally Cr was found to cover the Fe-rich substrate for the baffle in D, rust in E, and lid samples. This layer was occasionally porous. In general, more O was detected where Zn was depleted, and O and Cr were partly colocalised. Imaging by secondary electrons (SE) confirmed the heterogeneous quality of these layers. The Zn-enriched layer of the rust in the E sample contained distinct O-enriched, crystalline structures covered with a C-enriched sub-layer. Due to drift, the chemical analysis of the bottom in A sample was hard to interpret, but a thinner Zn-enriched layer was present here as well. The Zn-enriched layer was absent underneath the upper and lower biofilms in E. The biofilms themselves could be recognised by the presence of rounded structures with a diameter of 1–7 µm, enriched in C and O. These structures

Fig. 4 | Analysis of the carbon steel cross-section using metallography. Samples were embedded in resin, cut, and analysed via microscopy. This analysis not only gave an exact depth of the localised corrosion features but also the thickness of the steel plate. The shown sample from underneath the lower biofilm (bottom, right) was taken from a piece of bent steel, allowing colonisation on both sides, likely explaining the hole through the steel.

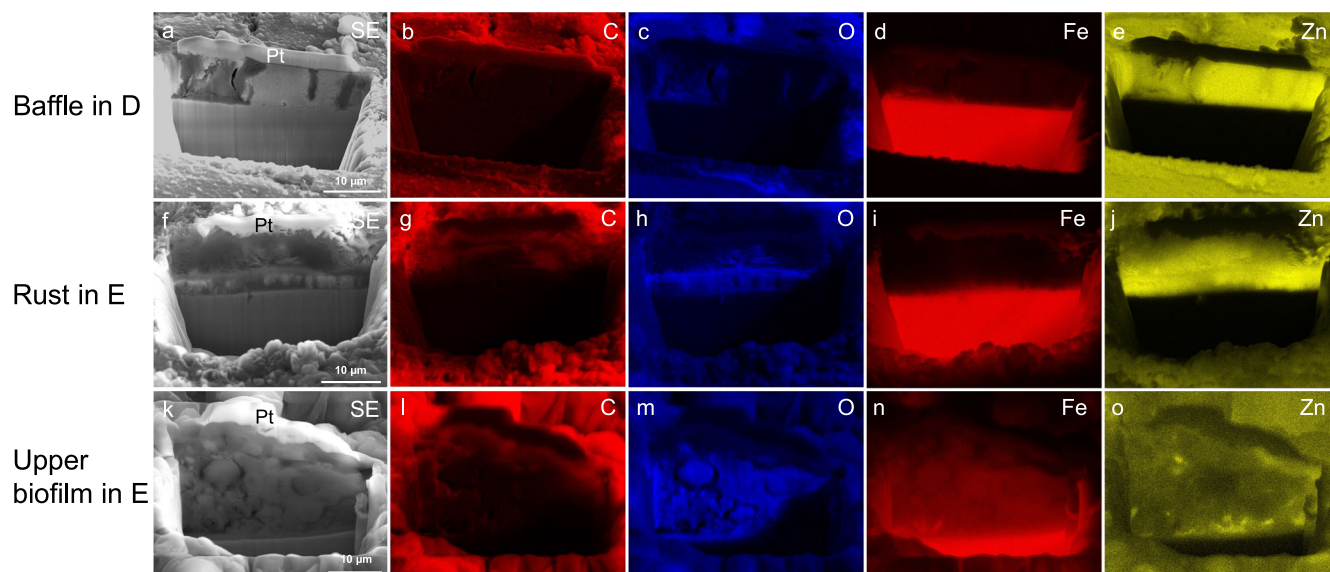
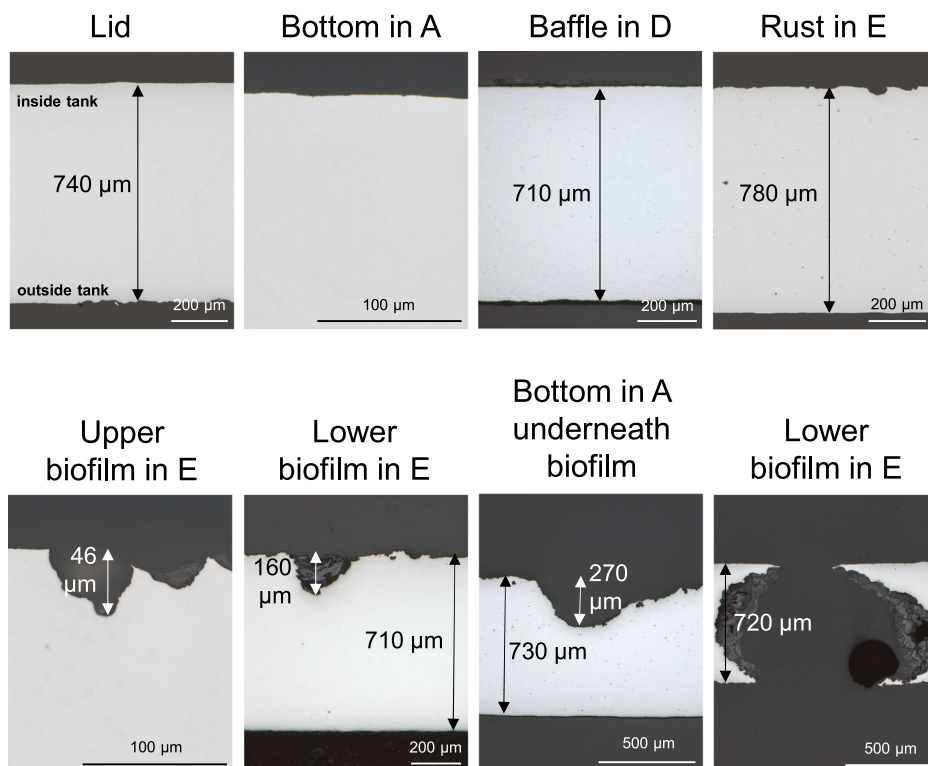


Fig. 5 | SEM-EDX analysis of metal samples prepared by FIB from the baffle in compartment D, the rust on compartment E and the upper biofilm in compartment E. a, f, k Secondary electron (SE) images of cross-sections obtained by FIB show the metal below covered by abiotic or biotic structures and a protective Pt

layer. b–e, g–j, l–o EDX maps of the same samples for selected elements. Note the presence of an ~10 μm thick layer enriched in Zn on top of the metal for the baffle and rust samples (e, j). This layer was absent underneath the upper biofilm (o).

were also slightly enriched in Fe and contained localised spots enriched in Zn.

Discussion

In this study, we used a multidisciplinary approach to examine the material of a 30-year-old diesel tank that had fouled in the fuel gauge, itself not an uncommon issue¹². We observed localised corrosion in the diesel tank underneath attached fungi-dominated biofilms. Both interferometric and

metallography analyses showed pits underneath the biofilm, but the depth of these was larger for the latter method, as interferometry does not allow the detection of the pit bottom of deeper pits. We therefore only discuss the depth of the pits observed by metallography. These results showed that up to 36% of the steel sheet was removed underneath biofilms (Fig. 4). Moreover, this observation was independent of the location, as it was done for biofilms grown in the main tank (compartment A) and in the fuel gauge compartment (E). Note that we do not take into account the hole observed in the

bent, inner sheet underneath the lower biofilm (Fig. 4) as we hypothesize that it was caused by the presence of fungal biofilms on both sides of the sheet. As the tank was in use for over 30 years, this is a case of modest microbiologically influenced corrosion (MIC). Some observations were nevertheless unexpected and need further discussion.

MIC or corrosion in general without the presence of a free water phase is rare. It is generally assumed that free water is needed for microbial growth and for corrosion to take place. For example, Wang et al.⁴², studied the corrosion of carbon steel submerged partly in tap water and partly in biodiesel, observing only the formation of iron oxide precipitates on the steel in contact with the water. However, since the introduction of biodiesel, more cases of corrosion have been noted in the vapour and fuel phase (i.e., the upper sections) of UST³¹. The saturation moisture content of biodiesel is 15–25 times higher than that of conventional petroleum diesel²⁷. The water content of FAME-based biodiesel was shown to be 150 ppm, higher than the 20 ppm measured for conventional diesel⁵. The water content of ~53 ppm in the biodiesel present in our tank (e.g., in compartment E) was relatively low compared to the data from Sørensen et al.⁵ and our sample of fresh biodiesel, which might have been caused by the extended storage of the tank at 4 °C. The fuel from this tank, nevertheless, likely contained more water than conventional diesel. Such high water contents not only allow for corrosion directly, but they also cause the hydrolysis of FAME, forming free fatty acids⁴³, omitting the need for free water.

Microbial biofilms dominated by *A. resiniae*, although ubiquitously and heterogeneously distributed on the tank surface, did not acidify the biodiesel nor cause an alteration of the biodiesel substrate (we did not use metabolite profiling to determine the deterioration of specific fuel components). We assume that these observations were caused by the high throughput of fuel prior to the storage at 4 °C in combination with a reduction in metabolic activity during the 4 °C incubation period. However, three isolates of *A. resiniae* retrieved from this tank were only able to reduce the pH when grown on B7 biodiesel from 6.00 pH units to 5.32, 5.92 and 4.16 pH units (Gerrits et al., in review), indicating that a general lack of acidification capacity may also explain our observations. Other fungi were also not capable of reducing the pH of diesel and biodiesel⁴⁴.

EDX mapping of the FIB cross-sections showed that the carbon steel samples, which were not covered with a biofilm, were coated with an ~10 µm thick Zn layer (note that Zn was absent in the OES results as this method analyses the bulk metal below the surface). Underneath biofilms, this coating was absent. Zn was also observed from above by ESEM and EDX; the hexagonal structures observed in the deposits for the rust in E and underneath E samples are indicative of Zn oxides (so-called wurtzite structures), and EDX analysis of these deposits showed that they were enriched in Zn. Zn coatings have been regularly applied to steel for over 200 years in a process called galvanisation⁴⁵. Such coatings aim to protect the underlying steel from corrosion by three mechanisms: (1) the formation of a barrier layer to avoid exposure to the environment, (2) galvanic protection whereby the Zn acts as a sacrificial anode, even protecting the underlying steel once the Zn coating is pierced and (3) upon dissolution, Zn will reprecipitate as an (hydr)oxide, forming a secondary barrier⁴⁵. Corrosion will preferentially take place at these porous Zn oxide sites, increasing linearly with time. Biodiesel by itself is only able to dissolve Zn coating at higher percentages (B20 or higher)^{46,47}, with pure biodiesel being corrosive to Zn (but not to carbon steel), releasing ca. 2.5 µg Zn g⁻¹ diesel after 28 days of incubation⁴⁸. This explains why, based on the absence of localised corrosion features in the biofilm-free samples (Fig. 4) in combination with the oxidised (i.e., O-enriched) and continuous (observed on the entire analysed surface) Zn coatings (Fig. 5), the Zn coatings effectively withstood abiotic corrosion, even after 30 years of operation of the diesel tank. It is impossible to know the timeframes in which the Zn coatings were removed by the biofilms, but the presence of considerable corrosion pits indicates their removal was accomplished quite some time ago. Future experimental work could determine the exact time needed for *A. resiniae* to corrode galvanised steel. Some Zn-enriched layers had a zone of Cr-enrichment (Supplementary Figs. 8 and 10). This Cr could have come from the underlying steel

(Supplementary Table 2), from the addition of Cr to the Zn galvanisation bath to inhibit Fe-Zn growth⁴⁹ or from the application of Cr coatings to protect the Zn coatings from wet-storage staining⁵⁰.

Underneath the biofilms, however, the coatings were notably absent, and only localised Zn-enriched sites were observed within the biofilms (Fig. 5). We therefore hypothesize that the biofilm-associated community members were responsible for the deterioration of the Zn coating.

Although many different prokaryotes identified by amplicon sequencing of the 16S rRNA gene were found in the diesel tank (Fig. 2b, Supplementary Fig. 1c), metagenome sequencing revealed that the community was predominantly comprised of fungi, with approximately 80% of the fungal reads belonging to *A. resiniae* (Supplementary Table 1). ESEM analysis (Fig. 3, Supplementary Fig. 4) also showed features of filamentous fungi similar in morphology to *A. resiniae* apart from the larger (20–30 µm), spherical structures, which were likely yeast cells covered in EPS. These capsules present a rather widespread adaptation among basidiomycetous yeasts that helps them to overcome unfavourable conditions and survive in extreme environments⁵¹. In general, ESEM imaging showed little to no evidence of the presence of bacterial cells (e.g., features that were 1–2 µm in size as would be typical for most bacteria)—this observation was further supported by the challenges (to date) in cultivating bacteria/archaea from the samples. The detection of prokaryotes at all sampling times, however, does indicate their presence in the diesel community, but currently, we can only speculate about where they may be located in the biofilm structures and their possible roles. For example, since they could not be observed by ESEM, it is possible that the prokaryotes in this system are completely encased within the fungal biomass, benefiting in some capacity from a synergistic relationship with the dominant fungus *A. resiniae*. Such fungal-bacterial relationships are widespread in nature⁵², though we are not aware of any interactions between *A. resiniae* and any specific bacteria inside or outside of the studied habitat. The high relative abundances of *Desulfovermiculus* and *Stenotrophomonas* in the 16S rRNA gene sequencing results could be caused by several factors. Even though there is no free water in the bulk liquid, it is possible that some free water with increased salt concentrations (not actually known) is present within the biofilms, thus osmotic stress tolerance might be at play. Both *Desulfovermiculus* and *Stenotrophomonas* genera have been associated with halotolerance^{53–56}; *Desulfovermiculus halophilus* was, for example, isolated from the salt-rich formation water of an oil field⁵⁴. Moreover, *Desulfovermiculus*, though a known SRB, and *Stenotrophomonas* have the ability to degrade organic compounds^{54,57}. Thus, it is feasible that members of both genera synergistically interact with *A. resiniae* or other community members in these capacities. This type of relationship has been suggested previously for bacteria-fungi kerosene communities based on the observation that the studied fungi could only grow on kerosene in the presence of their associated bacteria⁵⁸. However, other factors, like a higher expression of efflux pumps, might explain the presence of these bacteria as well⁵⁹. Consider as well that, based on the bacterial community shift from 2021 to 2022 (Supplementary Fig. 1), the prolonged incubation of the tank at 4 °C might explain the lower abundance of bacteria compared to fungi as observed in 2025.

In general, our observations agree with those of other studies where a free water phase in (bio)diesel was not detected or indicated during microbial corrosion tests. Stamps et al.³³ incubated uncoated and epoxy-coated carbon steel coupons in the upper and lower sections of B20 biodiesel-containing USTs located in the southern US. The differences between the bacterial communities were larger than between the fungal ones, and the coupons were covered with thick layers of hyphae³³, suggesting fungi were dominant. The authors, moreover, assumed the presence of free water (at the level of the lower coupons) but did not confirm this. An absence of such a phase could explain the absence of differences in the community composition of the lower and upper coupons³³. In another study, the microbial composition of the large water phase of diesel samples from Spanish ULSD storage tanks was dominated by bacteria⁶⁰. This confirms the general observation that SRB are only present in the water phase of diesel^{2,9}. Taken together, the low relative abundance of bacteria and archaea

in our diesel tank (as assessed by metagenome sequencing) is most likely due to the absence of a free water phase.

A. resinae was previously abundantly found in the diesel tanks of buses⁹, diesel storage tanks, and petrol station pumps². Moreover, fresh B7 diesel microbiologically analysed in this study was also dominated by *A. resinae* (Supplementary Fig. 1). This species, however, is not always dominant in a diesel-associated microbial community. For example, in diesel samples from tanks situated in Germany and Malaysia, *A. resinae* only comprised a marginal (<2%) part of the total fungal community (as determined via an *A. resinae*-specific qPCR test)²⁴. The USTs studied by Stamps et al.³³ were dominated by the fungus *P. dactylethromorphus*, *A. resinae* not being detected.

So why was the microbial community in the studied tank dominated by *A. resinae*? Compared to other fungi, *A. resinae* does not have a particularly high ability to biodegrade diesel¹⁴, thus other factors may have controlled its abundance in the diesel tank. (1) *A. resinae* might have a high ability to grow in water-deprived conditions. As discussed above, bacteria seem only able to grow on diesel in the presence of free water^{2,60}. Fungi are hypothesised to be more resistant to water deficiency as the internal transport in their hyphae makes them less dependent on water to deliver nutrients⁶¹. *A. resinae* has been shown to grow in kerosene with a water content of 80 ppm⁶². The metabolic degradation of hydrocarbons will result in the formation of so-called metabolic water⁶³. Indeed, after four weeks of incubation with kerosene containing 80 ppm water, *A. resinae* produced 0.94 g of water per litre of kerosene⁶². Note here that culturing attempts of *A. resinae* from this tank were successful (Gerrits et al., under review), indicating that the fungal biomass in this tank is viable. (2) Related to the water unavailability is osmotic stress: *A. resinae* might be dominant as it is capable to withstand the—potentially—high salt concentrations though the production of high concentrations of glycerol, the most common osmotic solute for fungi⁶⁴. (3) *A. resinae* could as well have inhibited growth of other species, as shown before for diesel-contaminating fungi⁶⁵, as few other fungal taxa were evident in the diesel tank (Fig. 2a, Supplementary Fig. 1b), aside from some round colonies covered in EPS. And lastly, (4) Zn, shown to be present as a coating on the carbon steel tank, is not only an essential nutrient for bacteria and fungi^{66,67}, but is also toxic at higher concentrations^{68,69}. Filamentous fungi are, for instance, affected by means of an increased chitin deposition in the cell wall, preventing hyphal extension, increasing hyphal branching and interfering with conidia development⁶⁸. These effects can be mitigated through storage of Zn in the vacuoles^{70,71}, its efflux⁷² and its binding by metallothionein-like peptides^{73,74}. Genes encoding Zn transporters (including efflux proteins) ascribed to *A. resinae* were detected in the metagenome of the diesel tank (Table 1). The same detection could not be done for metallothionein genes with a sufficient degree of certainty, likely due to their small size. Fomina et al.⁷⁵ showed how fungi grown on Zn phosphate precipitated large (up to 1 µm in diameter) Zn carboxylates in their hyphae, likely sacrificing some cells, as a detoxification strategy. Zn storage in the cell wall is assumed to be less pronounced for fungi^{70,76}. Melanin, however, is present in the cell wall of some fungi like *A. resinae*⁷⁷ (Gerrits et al., under review), and, based on the brown colour of the observed biofilms, produced in the studied conditions, is known to readily adsorb Zn⁷⁸. Moreover, Cu adsorbed to the melanin of *A. resinae* was best desorbed by Zn and Mg⁷⁹. To conclude, *A. resinae* likely dominated the diesel community in the studied tank by being able to grow in water-depleted conditions and its presumed tolerance to Zn.

We can only speculate as to how *A. resinae*-dominated biofilms enhanced the corrosion of galvanised carbon steel. The removal of the corrosion-inhibiting Zn layer (Fig. 5) certainly played a role, as a study of metallic Zn in contact with *Aspergillus niger* showed that this fungus was able to enhance the corrosion of Zn by decreasing the thickness of the protective Zn (hydr)oxide layer⁸⁰. These authors did not propose a mechanism that could explain their findings. A first possibility is fungal acidification. However, the bulk pH of diesel from the diesel tank was similar compared to fresh diesel and *A. resinae* isolates from this tank were not able to decrease the pH below 4 pH units (Gerrits et al., under review). Another

hypothesis is suggested by the patchy morphology of the observed biofilms. This phenomenon could enable the formation of an oxygen concentration cell: the area underneath the fungal biofilm is likely anoxic (as seen by Gerrits et al., under review), turning into an anode allowing localised corrosion¹⁹. Another possible mechanism is the relocation of Zn in the biofilm (in vacuoles, sacrificial hyphae, or melanin), lowering the Zn concentration at the biofilm-metal interface and driving Zn corrosion. Once the Zn coating has been pierced, the melanin of *A. resinae* could also enhance the corrosion of carbon steel, as shown by Gerrits et al. (under review). And finally, the mere production of metabolic water in the biofilm or the sorption of water by the biofilm would constitute the most straightforward corrosion mechanism. As corrosion of carbon steel is more severe for the steel surface that is in direct contact with water compared to biodiesel¹², simply enabling a constant presence of free water could drive corrosion underneath the biofilms. To conclude, even in the absence of free water, metabolically active *A. resinae*-dominated biofilms covered the galvanised steel of a 30-year-old diesel tank and caused considerable localised corrosion features. Elucidating the interactions between *A. resinae* and the prokaryotic community, along with controlled experiments assessing the corrosion of galvanised steel by this mixed community, remains a focus of future work to better understand the effects of microbial growth on fuel system materials designed to be inhibitory to corrosion.

Methods

Description of the tank and sampling procedure

In this work, we describe the multidisciplinary study of a fouled diesel tank of a Fiat Ducato I 280 campervan. The tank had a volume of 70 litres and dimensions of 750 by 820 by 230 cm. The tank had been in operation from 1989 to 2020, having likely been used with petroleum-based diesel (pre-2007), a B4.4 biodiesel blend (ca. 2007–2009), and B7 biodiesel (since ca. 2009), without known use of biocides. In 2020, the tank was removed and replaced due to fouling issues affecting the reliability of the fuel gauge and an insufficient fuel supply, leading to a loss of engine performance. When removing the tank connection with the intake hose and level sensor, a very heavy infestation of biofilm was found on the intake hose opening and level sensor. From 2020 to 2025, the tank was placed in a cool room at 4 °C and underwent recurrent sampling and isolation attempts. In 2021, the tank was opened in a non-destructive way in order to take images from inside the tank using an Olympus IV9435RX industrial videoscope (Supplementary Fig. 1a) and aseptically collect the first samples for microbial community sequencing. In 2022, new samples were taken for microbial sequencing, and first isolation attempts, both anaerobic and aerobic, were undertaken. The latter resulted in the successful isolation of three isolates of *A. resinae* (Gerrits et al., under review) but did not deliver any prokaryotic cultures. After it became clear that these isolates showed mixed results related to corrosion of carbon steel (in separate experiments, Gerrits et al., under review), we aimed to verify these results by analysing the microbial, chemical (fuel, water), and corrosion features of the tank.

In March 2025, the tank was fully opened using an electrical nibbler (Parkside) and we arbitrarily defined five compartments of interest (A to E, Fig. 1). The tank was divided in two by a baffle and on one side an extra steel compartment (designated compartment E) was welded onto the main body of the tank which contained the fuel gauge. The appearance of brown flocs and biofilm-like deposits (or lack thereof) within the tank guided the selection of samples for the analyses described in this study. The primary samples collected as 'background' samples, e.g., those that did not show visible evidence of flocs, debris, or biofilm included the lid (designated 'lid'), the bottom of compartment A (e.g., a section with no attached flocs, designated 'bottom in A'), and the baffle in compartment D (designated 'baffle in D'). The primary samples collected showing visible evidence of flocs, attached debris, or biofilm included the rust layer on a vertical wall of compartment E (designated 'rust in E'), the lower biofilm at the diesel-air interface in compartment E (designated 'lower biofilm in E'), the upper biofilm on contact area of compartment E and the baffle (designated 'upper biofilm in E'), and the area between compartment E and the main tank body

(see below for further description). Other samples that were subject to some analyses included the seam in C and loose flocs that were present in each of the five tank sections.

After opening and observing the tank, samples were first collected for molecular microbiological sequencing and cultivation. Liquid samples containing brown flocs were taken from the diesel present in each compartment (A through E), and initial swab samples were taken from the lid, rust in E, lower biofilm in E, upper biofilm in E, and seam in C.

The diesel layer in the tank was measured to be 23 mm deep, and no free water was visibly observed. Diesel samples for pH assessment, hydrocarbon/FAME component analysis and water content determination were taken from compartments A-C, compartment E, and from a sample obtained from a local gas station as a reference. Brown, unattached flocs were also sampled for microscopy and ESEM. Subsequently, all the diesel was removed, and the tank was further sectioned using the nibbler for additional analyses. During this sectioning process, a metal section under compartment E was discovered that also showed brown and pale-yellow slimy deposits - this section was also included in the primary floc/debris/biofilm sample set and was designated 'underneath E' (Fig. 1e). Samples were also collected from this newly exposed area for a variety of analyses.

The metal chemistry of the bulk of the main body of the tank (i.e., the lid) and the baffle was analysed using spark-OES. ESEM, focused ion beam FIB-EDX, and profilometry were performed on different metal samples with dimensions of ~10 by 10 mm, which were taken from the same locations. Samples from the lid, the rust in E, the lower and upper biofilm in E, the seam in C and the area underneath E, together with (as 'abiotic' controls) an area at the bottom of compartment A and on the baffle in compartment D, were prepared for ESEM. Profilometry was done for samples from the upper and lower biofilm in E, the rust in E, the lid, the baffle in D, the bottom in A, and underneath E. The upper and lower biofilm in E, the rust in E, the lid, the baffle in D, and the bottom in A samples were analysed by white light interferometry. Details about these various analyses are described below.

Diesel analysis

The diesel composition, the water content, and pH were determined for diesel samples taken from compartments A and E and a reference B7 diesel sample. The diesel composition was determined by diluting 4 mg of the respective diesel sample in 10 mL of *n*-heptane and submitting the mixture to gas chromatography with flame ionisation detection (GC-FID) on an 8890 Agilent gas chromatograph using a Restek MXT-1 capillary column (15 m × 0.28 mm × 0.1 µm; on-column injection of 2.5 µL) with helium as carrier gas. The oven temperature started at 60 °C (held 5 min) and was raised to 360 °C (40 °C/min). The detector temperature was set at 370 °C.

The water contents of the diesel samples were determined by means of Karl-Fischer titration on an 851 Titrand coulometer (Methrom) using a 34836 HYDRANAL™-Coulomat AG (Lot O1200) as anolyte, a 34840 HYDRANAL™-Coulomat™ CG (Lot M060J) as catholyte and a 34446 HYDRANAL Water Standard 0.10 PC (Lot K1770) as reference standard. A small volume (0.5 mL) of the respective diesel sample was directly dosed through the septum into the cell. Results are given as averages and the standard deviation of two independent analyses of the same sample.

The pH of the diesel samples taken from compartments A and E, and a reference B7 diesel sample, was estimated using pH-strips (ROTH) using aqueous extracts of the diesel.

Molecular microbiological methods

Samples for amplicon sequencing were collected from the tank in 2021, 2022, and 2025. For the 2021 and 2022 sampling, liquid samples were removed from an area near the bottom of the tank as well as near the surface of the diesel layer using sterile glass pipets (ca. 15 ml was sampled at each time point). One location was sampled in this manner, in duplicate (based on limited accessibility during non-destructive testing). Samples were placed into sterile conical tubes containing DNA/RNA ShieldTM (Zymo Research) to preserve the microbial community.

Once the tank was fully opened in 2025, additional samples were collected from several areas of the tank. Samples collected as liquids (using sterile pipets) included visible brown flocs from each of the assigned compartments, as well as a sample of the diesel itself in the tank. Swab samples were also collected from the lid (swabbing from a 35 × 10 cm area), upper biofilm in E, lower biofilm in E, rust in E, and from the seam in C (~20 cm length of the seam). Samples were amended with RNAlater[®] (ThermoFisher Scientific) to preserve the microbial community or transferred to sterile tubes for further cultivation experiments. When the tank was further cut for various analyses, the area under the fuel level compartment was exposed, and additional swab samples were collected from this location, designated underneath E, for amplicon sequencing. Further, this area, along with other attached brown debris attached to the metal at different locations on the tank surface, was swabbed as a representative sample for metagenomic sequencing. It should be noted that similar samples (loose flocs and attached debris/biofilm-like deposits) were also collected from the various compartments for culturing efforts of prokaryotes. For this purpose, samples were cultivated on medium M.830⁸¹ and incubated at ambient temperature either under aerobic, microaerophilic or anaerobic conditions for 3 months. Another cultivation attempt was made using medium M.382 lacking thiamine hydrochloride and glucose and supplemented with Wolin's vitamin solution (M.141⁸¹) and 0.01 ml ml⁻¹ of an autoclaved suspension of *A. resiniae* serving as an alternative carbon source. To control excessive fungal growth, both media were additionally supplemented with nystatin (0.05 mg ml⁻¹) and cycloheximide (0.05 mg ml⁻¹). In a third attempt, both media were additionally overlaid with 1 ml of sterile-filtered diesel. None of these attempts has been successful to date in culturing non-fungal microbial community members.

All samples were initially kept cold and then frozen at -20 °C until DNA extraction could be performed. DNA extractions were performed using the FastDNA™ Spin Kit for Soil (MPBiomedicals) according to the manufacturer's instructions, with a few deviations at the start of the procedure. Liquid samples were initially added to the Matrix E tubes, then treated with 100% isopropanol overnight to precipitate the DNA. Following centrifugation at 14,000 × g, the pellet was then washed with 70% ethanol and recentrifuged; the resulting pellet was transferred to the same Matrix E tube that was then processed as indicated in the kit. As much material as possible was removed from the swabs in the RNAlater[®] solution, which was then also centrifuged and reacted with 100% isopropanol for DNA precipitation. Following centrifugation, the pellet was washed in 70% ethanol, centrifuged again, and then transferred to a Matrix E tube that was then processed as directed by the manufacturer. Prior to PCR, recovered DNA from most samples was cleaned using the Zymo OneStep PCR Inhibitor Removal and DNA Clean & Concentrate kits (Zymo Research). For several samples, the entire process required repeating to obtain quantifiable DNA prior to carrying out the first PCR reaction. Some samples were also collected and processed in duplicate to determine reproducibility (rust in E, upper biofilm in E, underneath E). All samples were amplified using V4-V5 primers targeting bacteria/archaea⁸² and ITS primers targeting the ITS2 region in fungi (ITS3tagmix1 (forward) and ITS4ngs (reverse)⁸³, using thermocycling protocols from the cited references. Once quantifiable amounts of PCR product were obtained, a second PCR protocol⁸² was used to add barcodes for sequencing on an Illumina MiSeq at the Centre for Health Genomics and Informatics (University of Calgary, Canada).

Raw sequence reads were processed using an in-house pipeline that uses DADA2⁸⁴ in R. The processing pipeline included quality filtering of the raw reads, error correction, denoising, and chimera removal. Primers were removed from ITS2-amplified sequences using Cutadapt⁸⁵, and from 16S sequences using filterAndTrim (DADA2). Prokaryotic sequences (as ASVs, amplicon sequence variants) were identified by comparing against the SILVA 138.2 database⁸⁶, while ITS2 (fungal) sequences used the UNITE database⁸⁷ for taxonomic identification. Bubble plot visualisations were created using ggplot2, while NMDS (non-metric multi-dimensional scaling) plots (based on Bray-Curtis distance measures) to assess beta diversity were made using phyloseq⁸⁸.

The combined swab for metagenomic whole genome analysis was split into two equal pieces. The DNA extraction of one piece was done using the DNeasy PowerSoil Pro Kit (Qiagen) according to instructions. The second piece was treated using the procedure from Alibrandi et al.⁸⁹ that was successfully applied on oil samples by adding 10 µL SDS, and pre-heating to 65 °C for 10 min before bead beating using the DNeasy PowerSoil Pro Kit (Qiagen). Both extracts were pooled and cleaned using the Zymo OneStep PCR Inhibitor Removal DNA Clean & Concentrated kit (Zymo). The clean-up was sent for sequencing at CeGaT GmbH (Tübingen, Germany), aiming for 150 million Illumina read pairs of 2 × 100 bp length to potentially capture also low-abundance taxa. The sequencing resulted in 170,833,851 read pairs, which were processed using the ATLAS metagenome pipeline (v2.12)⁹⁰ to obtain quality-controlled reads, assembled contigs and functionally annotated genes. To obtain taxonomic and abundance information of the microbial community, the quality-controlled reads were mapped to the SILVA v138.1⁸⁶ and the UNITE fungi v8.3⁸⁷ database using Bowtie2 v2.3.4.1⁹¹ and Emu v3.5.1⁹². To verify eggNOG-annotated zinc transporter genes, BLAST⁹³ against the complete NCBI NT database (downloaded on 2025-10-04) was used.

Environmental scanning electron microscopy

Images of cut-out samples with and without thick biofilms and of floating biofilm flocs were obtained using an XL30 ESEM equipped with a tungsten cathode and a secondary electron detector (FEI/ThermoFisher Scientific). The quantitative analysis of the elemental composition of the surface structures was accomplished using a modular EDX system, Quantax 200, with an XFlash 6-60 silicon drift detector (Bruker Nano Analytics). Both ESEM and EDX analyses were undertaken in the “high-vacuum mode” of the microscope. EDX spectra were collected at an accelerating voltage of 20 keV. Due to the uneven sample surface morphology and the absence of standards, the elemental composition obtained via EDX must be considered as a rough estimate. The relative comparison of the results of different samples obtained under the same experimental conditions is more trustworthy than the absolute values obtained. Samples were prepared according to Spurr⁹⁴. Briefly, samples underwent a 2 h fixation using a 2.5% solution of glutaraldehyde in phosphate buffered saline (137 mM NaCl, 2.7 mM KCl, 10.1 mM Na₂HPO₄, 1.8 mM KH₂PO₄, pH set at 7.4), followed by dehydration via an ethanol dilution series (i.e., 30%, 50%, 70%, 80%, 90%, and absolute ethanol) and finally drying using critical point drying (Leica EM CPD300). All samples were coated with 30 nm gold prior to ESEM analysis. EDX analysis was conducted on select samples.

Determination of the bulk and surface chemistry of metal

The composition of the bulk of the metal was determined for two locations (the lid and the baffle) using a SPECTROLAB LAS01 (SPECTRO) spark-OES. Every sample was measured five times, and the averages are shown with one standard deviation of the mean.

Another batch of metal samples was removed from the same locations of the tank (the lid, rust in E, upper biofilm in E, lower biofilm in E, bottom in A, and the baffle in D) and immediately placed in a desiccator until preparation by focused ion beam scanning electron microscopy (FIB-SEM, 200xP, FEI/ThermoFisher Scientific). As thick biofilms are difficult to handle using this technique, most of the bulky biofilm was removed, leaving only the cells attached directly to the metal surface. Then an area of interest was defined, i.e., with an attached cell for the biofilm samples and with a seemingly clear surface for the other samples. A platinum layer (approximately 2.5 µm thick) was deposited on the area of interest using 30 kV gallium ion beam-induced deposition to protect the interface of interest from the high-energy gallium ions used for sputtering. A sample volume next to the area of interest was sputtered away using a gallium ion beam (30 kV, 3–30 nA) to obtain cross-sections, which were analysed by SEM at an angle of 52° to the surface (5 kV, secondary electron detector). EDX mapping was accomplished using a SDD Octane Elect Plus with an EDAX detector (Ametek) at 30 kV and 8 nA.

Quantification of surface pitting

The surface topography of a third batch of steel samples from equivalent locations was quantified to assess whether corrosion took place. For this purpose, we first removed the organic and inorganic deposits (e.g., biofilms) and then acquired a 5000 by 5000 µm map of the profile using a scanning white light interference microscope, Nexview (Zygo/AMETEK). A 10x Michelson interferometer objective was used with a lateral optical resolution of 0.95 µm and a vertical resolution of ~1–2 nm. For one sample (upper biofilm in E), an additional analysis was undertaken with a ×20 objective, obtaining a lateral resolution of 0.71 µm. The field-of-view was widened by using an internal optical zoom with ×0.5 and the stitching mode. The latter allows the linking of adjacent fields-of-view, with a defined overlap of 40%, into a large image of 5000 µm by 5000 µm. The depth of corrosion pits was quantified using single scanlines drawn within the region of interest and the OEM software Mx (Zygo). For each sample, the depth of the deepest pit was determined. The calibration and traceability are ensured by certified standards within a DIN EN ISO/IEC 17025:2018⁹⁵ accredited lab.

For metallography analysis, samples from three locations (rust in E, underneath biofilm in A, and underneath lower biofilm in E) were embedded in 2 K epoxy resin, cut with a wet cut grinding machine (ATM Brillant 250) and analysed using a Axioscope 7 (Zeiss) microscope.

Data availability

All data generated or analysed during this study are included in this published article [and its supplementary information].

Received: 16 July 2025; Accepted: 27 December 2025;

Published online: 16 January 2026

References

- Söhngen, N. Benzin, petroleum, paraffinöl und paraffin als kohlenstoff-und energiequelle für mikroben. *Zentr. Bakteriolog. Parasitenk. Abt. II* **37**, 595–609 (1913).
- Bento, F. M. & Gaylarde, C. C. Biodeterioration of stored diesel oil: studies in Brazil. *Int. Biodeterior. Biodegrad.* **47**, 107–112, [https://doi.org/10.1016/S0964-8305\(00\)00112-8](https://doi.org/10.1016/S0964-8305(00)00112-8) (2001).
- Edmonds, P. & Cooney, J. J. Identification of microorganisms isolated from jet fuel systems. *Appl. Microbiol.* **15**, 411–416, <https://doi.org/10.1128/am.15.2.411-416.1967> (1967).
- Komariah, L. N. et al. Microbial contamination of diesel-biodiesel blends in storage tank; an analysis of colony morphology. *Heliyon* **8**, e09264, <https://doi.org/10.1016/j.heliyon.2022.e09264> (2022).
- Sørensen, G., Pedersen, D. V., Nørgaard, A. K., Sørensen, K. B. & Nygaard, S. D. Microbial growth studies in biodiesel blends. *Bioresour. Technol.* **102**, 5259–5264, <https://doi.org/10.1016/j.biortech.2011.02.017> (2011).
- Schleicher, T., Werkmeister, R., Russ, W. & Meyer-Pittroff, R. Microbiological stability of biodiesel–diesel-mixtures. *Bioresour. Technol.* **100**, 724–730, <https://doi.org/10.1016/j.biortech.2008.07.029> (2009).
- da Fonseca, M. M. B. et al. Unlocking and functional profiling of the bacterial communities in diesel tanks upon additive treatment. *Fuel* **236**, 1311–1320, <https://doi.org/10.1016/j.fuel.2018.09.107> (2019).
- Marks, C. R. et al. An integrated metagenomic and metabolite profiling study of hydrocarbon biodegradation and corrosion in navy ships. *npj Mater. Degrad.* **5**, 60, <https://doi.org/10.1038/s41529-021-00207-z> (2021).
- Gaylarde, C. C., Bento, F. M. & Kelley, J. Microbial contamination of stored hydrocarbon fuels and its control. *Rev. Microbiol.* **30**, 01–10, <https://doi.org/10.1590/S0001-37141999000100001> (1999).
- Zobell, C. E. Action of microorganisms on hydrocarbons. *Bacteriol. Rev.* **10**, 1–49 (1946).
- Lansdown, A. R. Microbiological attack in aircraft fuel systems. *J. R. Aeronautical Soc.* **69**, 763–767, <https://doi.org/10.1017/S0368393100081694> (1965).

12. Passman, F. J. Microbial contamination and its control in fuels and fuel systems since 1980 – a review. *Int. Biodeterior. Biodegrad.* **81**, 88–104, <https://doi.org/10.1016/j.ibiod.2012.08.002> (2013).
13. Aktas, D. F. et al. Anaerobic hydrocarbon biodegradation and biocorrosion of carbon steel in marine environments: The impact of different ultra low sulfur diesels and bioaugmentation. *Int. Biodeterior. Biodegrad.* **118**, 45–56, <https://doi.org/10.1016/j.ibiod.2016.12.013> (2017).
14. Bento, F. M., Beech, I. B., Gaylarde, C. C., Englert, G. E. & Muller, I. L. Degradation and corrosive activities of fungi in a diesel–mild steel–aqueous system. *World J. Microbiol. Biotechnol.* **21**, 135–142, <https://doi.org/10.1007/s11274-004-3042-2> (2005).
15. Floyd, J. G., Stamps, B. W., Goodson, W. J. & Stevenson, B. S. Locating and quantifying carbon steel corrosion rates linked to fungal B20 biodiesel degradation. *Appl. Environ. Microbiol.* **87**, e0117721, <https://doi.org/10.1128/aem.01177-21> (2021).
16. Ching, T. H. et al. Biodegradation of biodiesel and microbiologically induced corrosion of 1018 steel by *Moniliella wahieum* Y12. *Int. Biodeterior. Biodegrad.* **108**, 122–126, <https://doi.org/10.1016/j.ibiod.2015.11.027> (2016).
17. Aslan, C., Aulia, N. I., Devianto, H. & Harimawan, A. Influence of axenic culture of *Bacillus clausii* and mixed culture on biofilm formation, carbon steel corrosion, and methyl ester degradation in B30 storage tank system. *J. Environ. Chem. Eng.* **10**, 108013, <https://doi.org/10.1016/j.jece.2022.108013> (2022).
18. Xu, D., Gu, T. & Lovley, D. R. Microbially mediated metal corrosion. *Nat. Rev. Microbiol.* **21**, 705–718, <https://doi.org/10.1038/s41579-023-00920-3> (2023).
19. Knisz, J. et al. Microbiologically influenced corrosion—more than just microorganisms. *FEMS Microbiol. Rev.* **47**, fuad041 (2023).
20. Khan, S. et al. Harnessing bacterial power: advanced strategies and genetic engineering insights for biocorrosion control and inhibition. *npj Mater. Degrad.* **9**, 74, <https://doi.org/10.1038/s41529-025-00623-5> (2025).
21. Luz, G. V. S., Sousa, B. A. S. M., Guedes, A. V., Barreto, C. C. & Brasil, L. M. Biocides used as additives to biodiesels and their risks to the environment and public health: a review. *Molecules* **23**, 2698, <https://doi.org/10.3390/molecules23102698> (2018).
22. Bailey, C. A. & May, M. E. Evaluation of microbiological test kits for hydrocarbon fuel systems. *Appl. Environ. Microbiol.* **37**, 871–877, <https://doi.org/10.1128/aem.37.5.871-877.1979> (1979).
23. Lopes, P. T. C. & Gaylarde, C. Use of immunofluorescence to detect the fungus *Hormoconis resiniae* in aviation kerosine. *Int. Biodeterior. Biodegrad.* **37**, 37–40, [https://doi.org/10.1016/0964-8305\(95\)00110-7](https://doi.org/10.1016/0964-8305(95)00110-7) (1996).
24. Martin-Sanchez, P. M., Gorbushina, A. A., Kunte, H. J. & Toepel, J. A novel qPCR protocol for the specific detection and quantification of the fuel-deteriorating fungus *Hormoconis resiniae*. *Biofouling* **32**, 635–644, <https://doi.org/10.1080/08927014.2016.1177515> (2016).
25. Bückner, F. et al. Evaluation of the detriogenic microbial community using qPCR, n-alkanes and FAMES biodegradation in diesel, biodiesel and blends (B5, B10, and B50) during storage. *Fuel* **233**, 911–917, <https://doi.org/10.1016/j.fuel.2017.11.076> (2018).
26. Amsellem, D. et al. *Perspectives d'évolution des biocarburants: jeux des acteurs et enjeux fonciers*. (L'Observatoire de la sécurité des flux et des matières énergétiques, 2021).
27. He, B. B., Thompson, J. C., Routt, D. W. & Van Gerpen, J. H. Moisture absorption in biodiesel and its petro-diesel blends. *Appl. Eng. Agric.* **23**, 6, <https://doi.org/10.13031/2013.22320> (2007).
28. Dodos, G., Konstantakos, T., Longinos, S. & Zannikos, F. Effects of microbiological contamination in the quality of biodiesel fuels. *Glob. NEST J.* **14**, 175–182, <https://doi.org/10.30955/gnj.000856> (2012).
29. Lee, J. S., Ray, R. I. & Little, B. J. An assessment of alternative diesel fuels: microbiological contamination and corrosion under storage conditions. *Biofouling* **26**, 623–635, <https://doi.org/10.1080/08927014.2010.504984> (2010).
30. Lyles, C. N. et al. Impact of organosulfur content on diesel fuel stability and implications for carbon steel corrosion. *Environ. Sci. Technol.* **47**, 6052–6062, <https://doi.org/10.1021/es4006702> (2013).
31. EPA, U. *Investigation Of Corrosion-Influencing Factors In Underground Storage Tanks With Diesel Service*. EPA 510-R-16-001. (United States Environmental Protection Agency, 2016).
32. Houbraken, J., Visagie Cobus, M. & Frisvad Jens, C. Recommendations to prevent taxonomic misidentification of genome-sequenced fungal strains. *Microbiol. Resour. Announc.* **10**, e01074–01020, <https://doi.org/10.1128/MRA.01074-20> (2021).
33. Stamps, B. W. et al. In situ linkage of fungal and bacterial proliferation to microbiologically influenced corrosion in B20 biodiesel storage tanks. *Front. Microbiol.* **11**, 167, <https://doi.org/10.3389/fmicb.2020.00167> (2020).
34. Cofone, L., Walker, J. D. & Cooney, J. J. Utilization of hydrocarbons by *Cladosporium resiniae*. *Microbiology* **76**, 243–246, <https://doi.org/10.1099/00221287-76-1-243> (1973).
35. Lindley, N. D. & Heydeman, M. T. The uptake of n-alkanes from alkane mixtures during growth of the hydrocarbon-utilizing fungus *Cladosporium resiniae*. *Appl. Microbiol. Biotechnol.* **23**, 384–388, <https://doi.org/10.1007/BF00257038> (1986).
36. Krivushina, A. A., Bobyrev, T. V. & Mokeeva, V. L. Growth ability of “kerosene fungus” *Amorphotheca resiniae* strains isolated from different habitats in aviation fuel. *Biol. Bull. Rev.* **13**, S93–S98, <https://doi.org/10.1134/S2079086423070095> (2023).
37. Parbery, D. G. *The Kerosene Fungus, Amorphotheca resiniae: Its Biology, Taxonomy and Control*. (University of Melbourne, 1970).
38. Krohn, I. et al. Deep (meta)genomics and (meta)transcriptome analyses of fungal and bacteria consortia from aircraft tanks and kerosene identify key genes in fuel and tank corrosion. *Front. Microbiol.* **12**, 722259 (2021).
39. Walker, J. D. & Cooney, J. J. Aliphatic hydrocarbons of *Cladosporium resiniae* cultured on glucose, glutamic acid, and hydrocarbons. *Appl. Microbiol.* **26**, 705–708, <https://doi.org/10.1128/am.26.5.705-708.1973> (1973).
40. Schirmer, M. et al. Insight into biases and sequencing errors for amplicon sequencing with the Illumina MiSeq platform. *Nucleic Acids Res.* **43**, e37–e37, <https://doi.org/10.1093/nar/gku1341> (2015).
41. Martino, E. et al. Comparative genomics and transcriptomics depict ericoid mycorrhizal fungi as versatile saprotrophs and plant mutualists. *N. Phytol.* **217**, 1213–1229, <https://doi.org/10.1111/nph.14974> (2018).
42. Wang, W., Jenkins, P. E. & Ren, Z. Heterogeneous corrosion behaviour of carbon steel in water contaminated biodiesel. *Corros. Sci.* **53**, 845–849, <https://doi.org/10.1016/j.corsci.2010.10.020> (2011).
43. Fang, H. L. & McCormick, R. L. Spectroscopic study of biodiesel degradation pathways. *SAE Technical Paper 2006-01-3300* (2006).
44. Bückner, F. et al. Impact of biodiesel on biodeterioration of stored Brazilian diesel oil. *Int. Biodeterior. Biodegrad.* **65**, 172–178, <https://doi.org/10.1016/j.ibiod.2010.09.008> (2011).
45. Marder, A. R. The metallurgy of zinc-coated steel. *Prog. Mater. Sci.* **45**, 191–271, [https://doi.org/10.1016/S0079-6425\(98\)00006-1](https://doi.org/10.1016/S0079-6425(98)00006-1) (2000).
46. Ku, Y.-Y., Tang, T.-W., Lin, K. W. & Chan, S. The impact upon applicability of metal fuel tank using different biodiesel. *SAE Int. J. Mater. Manuf.* **8**, 757–764, <https://doi.org/10.4271/2015-01-0521> (2015).
47. Ackermann, H. et al. *Entwicklung einer Prüfmethode zur Bewertung der Materialbeständigkeit von Bauteilen in Mitteldestillatanwendungen*. (DGfM, 2020).
48. Fernandes, D. M. et al. Storage stability and corrosive character of stabilised biodiesel exposed to carbon and galvanised steels. *Fuel* **107**, 609–614, <https://doi.org/10.1016/j.fuel.2012.11.010> (2013).

49. Mackowiak, J. & Short, N. R. Metallurgy of galvanized coatings. *Int. Met. Rev.* **24**, 1–19, <https://doi.org/10.1179/imtr.1979.24.1.1> (1979).
50. Townsend, H. & Hart, R. Composition of chromate passivation films on aluminum–zinc alloy–coated sheet steel. *J. Electrochem. Soc.* **131**, 1345–1348, <https://doi.org/10.1149/1.2115817> (1984).
51. Buzzini, P., Turchetti, B. & Yurkov, A. Extremophilic yeasts: the toughest yeasts around? *Yeast* **35**, 487–497, <https://doi.org/10.1002/yea.3314> (2018).
52. Deveau, A. et al. Bacterial–fungal interactions: ecology, mechanisms and challenges. *FEMS Microbiol. Rev.* **42**, 335–352, <https://doi.org/10.1093/femsre/fuy008> (2018).
53. Alexander, A., Singh, V. K. & Mishra, A. Halotolerant PGPR *Stenotrophomonas maltophilia* BJ01 induces salt tolerance by modulating physiology and biochemical activities of *Arachis hypogaea*. *Front. Microbiol.* **11**, 568289 (2020).
54. Belyakova, E. V. et al. The new facultatively chemolithoautotrophic, moderately halophilic, sulfate-reducing bacterium *Desulfovermiculus halophilus* gen. nov., sp. nov., isolated from an oil field. *Microbiology* **75**, 161–171, <https://doi.org/10.1134/S0026261706020093> (2006).
55. Oren, A. Thermodynamic limits to microbial life at high salt concentrations. *Environ. Microbiol.* **13**, 1908–1923, <https://doi.org/10.1111/j.1462-2920.2010.02365.x> (2011).
56. Steinle, L. et al. Life on the edge: active microbial communities in the Kryos MgCl₂-brine basin at very low water activity. *Isme J.* **12**, 1414–1426, <https://doi.org/10.1038/s41396-018-0107-z> (2018).
57. Ryan, R. P. et al. The versatility and adaptation of bacteria from the genus *Stenotrophomonas*. *Nat. Rev. Microbiol.* **7**, 514–525, <https://doi.org/10.1038/nrmicro2163> (2009).
58. Shapiro, T. et al. Revealing of non-cultivable bacteria associated with the mycelium of fungi in the kerosene-degrading community isolated from the contaminated jet fuel. *J. Fungi* **7**, 43, <https://doi.org/10.3390/jof7010043> (2021).
59. Gunasekera, T. S., Striebich, R. C., Mueller, S. S., Strobel, E. M. & Ruiz, O. N. Transcriptional profiling suggests that multiple metabolic adaptations are required for effective proliferation of *Pseudomonas aeruginosa* in jet fuel. *Environ. Sci. Technol.* **47**, 13449–13458, <https://doi.org/10.1021/es403163k> (2013).
60. Martin-Sanchez, P. M., Gorbushina, A. A. & Toepel, J. Quantification of microbial load in diesel storage tanks using culture- and qPCR-based approaches. *Int. Biodeterior. Biodegrad.* **126**, 216–223, <https://doi.org/10.1016/j.ibiod.2016.04.009> (2018).
61. Prenafeta-Boldú, F. X., de Hoog, G. S. & Summerbell, R. C. in *Microbial Communities Utilizing Hydrocarbons and Lipids* (ed McGenity, T. J.) 307–342 (Springer, 2019).
62. Hill, E. & Thomas, A. in *Proceedings of the Third International Biodegradation Symposium* 157–174 (1977).
63. van Beilen, J. B. & Funhoff, E. G. Alkane hydroxylases involved in microbial alkane degradation. *Appl. Microbiol. Biotechnol.* **74**, 13–21, <https://doi.org/10.1007/s00253-006-0748-0> (2007).
64. Gunde-Cimerman, N., Plemenitaš, A. & Oren, A. Strategies of adaptation of microorganisms of the three domains of life to high salt concentrations. *FEMS Microbiol. Rev.* **42**, 353–375, <https://doi.org/10.1093/femsre/fuy009> (2018).
65. Hettige, G. E. G. & Sheridan, J. E. Interactions of fungi contaminating diesel fuel. *Int. Biodeterior.* **25**, 299–309, [https://doi.org/10.1016/0265-3036\(89\)90004-3](https://doi.org/10.1016/0265-3036(89)90004-3) (1989).
66. Gerwien, F., Skrahina, V., Kasper, L., Hube, B. & Brunke, S. Metals in fungal virulence. *FEMS Microbiol. Rev.* **42**, fux050 (2017).
67. Lonergan, Z. R. & Skaar, E. P. Nutrient zinc at the host–pathogen interface. *Trends Biochem. Sci.* **44**, 1041–1056, <https://doi.org/10.1016/j.tibs.2019.06.010> (2019).
68. Robinson, J. R., Isikhuemhen, O. S. & Anike, F. N. Fungal–metal interactions: a review of toxicity and homeostasis. *J. Fungi* **7**, 225, <https://doi.org/10.3390/jof7030225> (2021).
69. McDevitt, C. A. et al. A molecular mechanism for bacterial susceptibility to zinc. *PLoS Pathog.* **7**, e1002357, <https://doi.org/10.1371/journal.ppat.1002357> (2011).
70. Simm, C. et al. *Saccharomyces cerevisiae* vacuole in zinc storage and intracellular zinc distribution. *Eukaryot. Cell* **6**, 1166–1177, <https://doi.org/10.1128/ec.00077-07> (2007).
71. Cho, M. et al. Vacuolar zinc transporter Zrc1 is required for detoxification of excess intracellular zinc in the human fungal pathogen *Cryptococcus neoformans*. *J. Microbiol.* **56**, 65–71, <https://doi.org/10.1007/s12275-018-7475-y> (2018).
72. Ruytinx, J. et al. Zinc export results in adaptive zinc tolerance in the ectomycorrhizal basidiomycete *Suillus bovinus*. *Metallomics* **5**, 1225–1233, <https://doi.org/10.1039/c3mt00061c> (2013).
73. Leonhardt, T., Sácký, J., Šimek, P., Šantrůček, J. & Kotrba, P. Metallothionein-like peptides involved in sequestration of Zn in the Zn-accumulating ectomycorrhizal fungus *Russula atropurpurea*. *Metallomics* **6**, 1693–1701, <https://doi.org/10.1039/c4mt00141a> (2014).
74. Kalsotra, T., Khullar, S., Agnihotri, R. & Reddy, M. S. Metal induction of two metallothionein genes in the ectomycorrhizal fungus *Suillus himalayensis* and their role in metal tolerance. *Microbiology* **164**, 868–876, <https://doi.org/10.1099/mic.0.000666> (2018).
75. Fomina, M., Charnock, J., Bowen, A. D. & Gadd, G. M. X-ray absorption spectroscopy (XAS) of toxic metal mineral transformations by fungi. *Environ. Microbiol.* **9**, 308–321, <https://doi.org/10.1111/j.1462-2920.2006.01139.x> (2007).
76. Kleijburg, F. E. L., Safeer, A. A., Baldus, M. & Wösten, H. A. B. Binding of micro-nutrients to the cell wall of the fungus *Schizophyllum commune*. *Cell Surf.* **10**, 100108, <https://doi.org/10.1016/j.tcsu.2023.100108> (2023).
77. San-Blas, G., Guanipa, O., Moreno, B., Pekarar, S. & San-Blas, F. *Cladosporium carrionii* and *Hormoconis resiniae* (C. *resiniae*): Cell wall and melanin studies. *Curr. Microbiol.* **32**, 11–16, <https://doi.org/10.1007/s002849900003> (1996).
78. Fogarty, R. V. & Tobin, J. M. Fungal melanins and their interactions with metals. *Enzym. Microb. Technol.* **19**, 311–317, [https://doi.org/10.1016/0141-0229\(96\)00002-6](https://doi.org/10.1016/0141-0229(96)00002-6) (1996).
79. Gadd, G. M. & Derome, L. Biosorption of copper by fungal melanin. *Appl. Microbiol. Biotechnol.* **29**, 610–617, <https://doi.org/10.1007/BF00260993> (1988).
80. Juzeliūnas, E. et al. Microbially influenced corrosion of zinc and aluminium – two-year subjection to influence of *Aspergillus niger*. *Corros. Sci.* **49**, 4098–4112, <https://doi.org/10.1016/j.corsci.2007.05.004> (2007).
81. Koblitz, J. et al. MediaDive: the expert-curated cultivation media database. *Nucleic Acids Res.* **51**, D1531–D1538, <https://doi.org/10.1093/nar/gkac803> (2022).
82. Rachel, N. M. & Gieg, L. M. Preserving microbial community integrity in oilfield produced water. *Front. Microbiol.* **11**, 581387 (2020).
83. Tedersoo, L. et al. Shotgun metagenomes and multiple primer pair-combinations of amplicons reveal biases in metabarcoding analyses of fungi. *MycKeys* **10**, 4852 (2015).
84. Callahan, B. J. et al. DADA2: High-resolution sample inference from Illumina amplicon data. *Nat. Methods* **13**, 581–583, <https://doi.org/10.1038/nmeth.3869> (2016).
85. Martin, M. Cutadapt removes adapter sequences from high-throughput sequencing reads. *EMBnet* **17**, 3, <https://doi.org/10.14806/ej.17.1.200> (2011).
86. Quast, C. et al. The SILVA ribosomal RNA gene database project: improved data processing and web-based tools. *Nucleic Acids Res.* **41**, D590–D596, <https://doi.org/10.1093/nar/gks1219> (2012).
87. Abarenkov, K. et al. The UNITE database for molecular identification and taxonomic communication of fungi and other eukaryotes: sequences, taxa and classifications reconsidered. *Nucleic Acids Res.* **52**, 791–797, <https://doi.org/10.1093/nar/gkad1039> (2023).

88. McMurdie, P. J. & Holmes, S. phyloseq: an R package for reproducible interactive analysis and graphics of microbiome census data. *Plos One* **8**, e61217, <https://doi.org/10.1371/journal.pone.0061217> (2013).
89. Alibrandi, A., di Primio, R., Bartholomäus, A. & Kallmeyer, J. A modified iso-octane-based DNA extraction method from crude oil. *mLife* **2**, 328–338, <https://doi.org/10.1002/mlf2.12081> (2023).
90. Kieser, S., Brown, J., Zdobnov, E. M., Trajkovski, M. & McCue, L. A. ATLAS: a snakemake workflow for assembly, annotation, and genomic binning of metagenome sequence data. *BMC Bioinform.* **21**, 257, <https://doi.org/10.1186/s12859-020-03585-4> (2020).
91. Langmead, B. & Salzberg, S. L. Fast gapped-read alignment with Bowtie 2. *Nat. Methods* **9**, 357–359, <https://doi.org/10.1038/nmeth.1923> (2012).
92. Curry, K. D. et al. Emu: species-level microbial community profiling of full-length 16S rRNA Oxford Nanopore sequencing data. *Nat. Methods* **19**, 845–853, <https://doi.org/10.1038/s41592-022-01520-4> (2022).
93. Camacho, C. et al. BLAST+: architecture and applications. *BMC Bioinform.* **10**, 421, <https://doi.org/10.1186/1471-2105-10-421> (2009).
94. Spurr, A. R. A low-viscosity epoxy resin embedding medium for electron microscopy. *J. Ultrastruct. Res.* **26**, 31–43, [https://doi.org/10.1016/S0022-5320\(69\)90033-1](https://doi.org/10.1016/S0022-5320(69)90033-1) (1969).
95. DIN. *EN ISO/IEC 17025:2018-03, General requirements for the competence of testing and calibration laboratories.* (2018).
- provision of the fuel tank for study; supplying comprehensive information on the tank failure and the vehicle's 30-year operational history; J.S.: analysis of fungal biology and genomes; A.A.G.: conceptualisation; sampling, SEM analysis, funding acquisition; L.M.G.: conceptualisation, sampling, SEM analysis, writing original draft, funding acquisition. Writing – review & editing: all co-authors.

Funding

Open Access funding enabled and organized by Projekt DEAL.

Competing interests

The authors declare no competing interests.

Additional information

Supplementary information The online version contains supplementary material available at <https://doi.org/10.1038/s41529-025-00731-2>.

Correspondence and requests for materials should be addressed to Lisa M. Gieg or Anna A. Gorbushina.

Reprints and permissions information is available at <http://www.nature.com/reprints>

Publisher's note Springer Nature remains neutral with regard to jurisdictional claims in published maps and institutional affiliations.

Open Access This article is licensed under a Creative Commons Attribution 4.0 International License, which permits use, sharing, adaptation, distribution and reproduction in any medium or format, as long as you give appropriate credit to the original author(s) and the source, provide a link to the Creative Commons licence, and indicate if changes were made. The images or other third party material in this article are included in the article's Creative Commons licence, unless indicated otherwise in a credit line to the material. If material is not included in the article's Creative Commons licence and your intended use is not permitted by statutory regulation or exceeds the permitted use, you will need to obtain permission directly from the copyright holder. To view a copy of this licence, visit <http://creativecommons.org/licenses/by/4.0/>.

© The Author(s) 2026

Acknowledgements

This study was supported by internal funds of the B.A.M., with amplicon sequencing supported by NSERC Discovery and Genome Canada grants awarded to L.M.G. We thank Alexander Bartholomäus of GreenGate Genomics for the metagenomic whole genome analysis.

Author contributions

R.G.: sampling and sample preparation, data acquisition, curation, visualisation, writing original draft; A.Y.: analysis of fungal SEM images and sequencing data; I.F. conducted ESEM and EDX analyses; M.D., U.K.: technical support, sample preparation; M.N.S., J.W., S.K., B.A.S.: aseptic sampling, isolation of prokaryotes; Ra.Bä.: corrosion methodology and data analysis; R.H., A.H., M.W., T.M., H.S., Y.S., N.M.T., K.L.G.: sample treatment and data acquisition; Ro.Be.: diesel expertise, data analysis; O.O.: conceptualisation, corrosion analysis; J.G.: detection of the corrosion case,